I.J. Image, Graphics and Signal Processing, **2024, 6, 17-31**
Published Online on December 8, 2024 by MECS Press (http://www.mecs-press.org/)
DOI: 10.5815/ijigsp.2024.06.02

Glaucoma Detection and Severity Diagnosis from Fundus Images Using Dual CNN Architectures

G. Latha
Department of Electronics and Communication Engineering, SRM Institute of Science and Technology, Kattankulathur-603203, Chengalpattu District, Tamil Nadu, India
E-mail: lg3046@srmist.edu.in
ORCID iD: https://orcid.org/0009-0006-2034-0645

P. Aruna Priya*
Department of Electronics and Communication Engineering, SRM Institute of Science and Technology, Kattankulathur-603203, Chengalpattu District, Tamil Nadu, India
Email: arunaprp@srmist.edu.in
ORCID iD: https://orcid.org/0000-0002-5612-3312
*Corresponding Author

Received: 30 October, 2023; Revised: 16 December, 2023; Accepted: 23 February, 2024; Published: 08 December, 2024

Abstract: Glaucoma, a series of progressive eye illnesses, is a primary worldwide health concern. Glaucoma, sometimes known as the "silent thief of sight," progressively affects the optic nerve, resulting in permanent vision loss and, in extreme instances, blindness. It is essential to recognize glaucoma in its earlier stages so that patients can receive treatment sooner and prevent further vision loss. An effective method for detecting glaucoma by analyzing retinal images with the assistance of a deep learning strategy is presented as a potential solution in this article. The framework presented for detecting glaucoma comprises two modules that rely on one another: the Retinal Image Classification Module (RICM) and the Retinal Image Diagnosis Module (RIDM). The retinal image is classified as either a normal or a glaucoma retinal image by the RICM module, which uses the CNN classifier. The RIDM detects the neuro rim region from the glaucoma retinal image by segmenting OD and OC, and the Dual Functional CNN (DFCNN) classifier is proposed to diagnose the severity stages of the glaucoma image based on the feature patterns that are extracted from the neuroretinal rim in the glaucoma image. Both low- and high-resolution retinal image datasets, known as HRF and PAPILA, are utilized in this study to investigate the proposed approaches for glaucoma identification and severity estimate. Compared to other methods considered to be state-of-the-art, the simulation's findings show that it is successful. Ophthalmologists benefit from the suggested model since it assists them in effectively recognizing glaucoma in patients, which in turn allows for improved diagnosis and the prevention of premature vision loss.

Index Terms: Glaucoma, Optic disk, Optic cup, retinal rim, YOLO.

1. Introduction

Glaucoma is a potentially blinding disease but fortunately preventable and preventing from progression if detected early. It is multifactorial. Intraocular pressure (IOP) is the only controllable factor at present. Measuring and detecting neuroretinal rim and retinal nerve fiber layer changes are the key factors in detecting and diagnosing glaucoma. The incidence of Primary Open Angle Glaucoma (POAG) in our country is 0.6%, meaning 6.48 million persons are affected by it. It is more common than Angle Closure Glaucoma. POAG being asymptomatic, gets delayed till irreversible damage has occurred. Hence the use of Artificial Intelligence in detecting early changes in fundus can help the burden of blindness due to glaucoma in our country. The human eye is a symbol of the signs and symptoms of a variety of diseases that can affect the human body. Therefore, research on the human eye should be conducted appropriately to provide solutions for the numerous eye-related ailments that affect the human body. As shown in Figure 1, the retina of the human eye is made up of three major components: the macula, the optic disc (OD), and the optic cup (OC). Additionally, the retina contains blood vessels. The blood arteries of the retina are said to have begun from the center of the OC and expanded out to all areas of the retina. The portion of the retina with the strongest intensity is called the OD, and the brightest region inside the OD is called the OC. In contrast to the OD and OC areas, the macula is characterized

by a relatively low level of light intensity in the retina. The fovea, located at the center of the macula, has no retinal blood vessels running through it. Diseases affecting the eye can be identified and diagnosed through observation of the anatomical components contained within a picture of the retina. Analyzing the pictures of the retinal fundus can serve as a screening method for several eye illnesses, including the well-known diabetic retinopathy (DR) and glaucoma. Damage to the retinal blood vessels is the root cause of diabetic retinopathy, whereas damage to the OD and OC areas of the retinal images is the root cause of glaucoma [1,2].

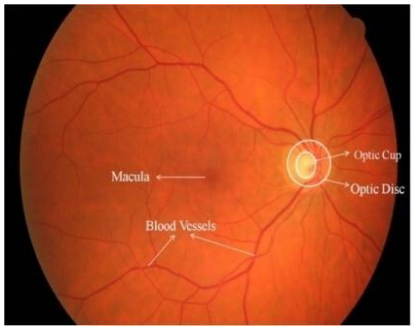

Fig. 1. Internal structure of the retinal image-HRF Dataset

One of the most widely used screening tests for glaucoma is the Cup-to-Disc ratio (CDR) of the optic nerve head, which compares the vertical diameter of the optic cup to that of the disc [3]. If the CDR value is less than 0.5, the eye is considered healthy; if it is more than or equal to 0.5, the eye is considered glaucoma-infected [4]. Based on the Ensemble, a Spatially Based Ellipse Fitting Curve Model (SBEFCM) classification [5] is proposed for an accurate diagnosis of Glaucoma in the Optic Cup (OC) and Optic Disc (OD) border. LAG and RIM-ONE databases were utilized in this suggested investigation to identify glaucoma. The LAG database has higher accuracy than the RIM-ONE dataset.

The practical application of this paper is to bring a fully automated computer-aided process for Glaucoma retinal image detection and classifications which helps ophthalmologists to screen Glaucoma in large population countries such as India.

The fundamental purpose of this study is to create a computer-assisted glaucoma detection system making use of deep learning techniques. Using the suggested YOLO architecture, this technique identifies and classifies the retinal images as either Glaucoma or non-glaucoma. After that, the categorized Glaucoma retina image is diagnosed as either "Early" or "Advanced" utilizing Dual Convolutional Neural Networks (CNN) deep learning methods. The performance of the established Glaucoma detection framework model was assessed by applying the proposed methodologies to both low-intensity and high-intensity retinal image datasets.

The outline of the work that has been proposed is as follows:

- Image augmentation is applied to the fundus image to generate additional images for use in training the model.
- Following the augmentation of the image, the YOLO-V5 CNN architecture was trained using the image data set.
- During the third step, the YOLO-V5 CNN architecture was used to extract the deep learning matrix.
- During the testing phase, the features that were learned by deep learning were utilized to classify the images as either healthy or glaucoma.
- Using the anisotropic diffusion method, the neuroretinal rim was segmented from the glaucoma images.
- Finally, glaucoma fundus pictures were categorized using Dual Functional CNN (DFCNN) to determine whether they belonged to the early or advanced phases of the disease.

This article is broken up into a few different sections. Module 2 of the proposal presents a complete evaluation of important literature related to Glaucoma detection. Module 3 describes the Glaucoma detection methods used in this study. In Module 4, the experimental findings of the proposed model are compared to those of conventional approaches. Finally, Module 5 summarises the study's conclusions and findings.

2. Related Works on Glaucoma Detection

The development of advanced glaucoma detection systems has been driven by significant developments in medical imaging, computer vision, and machine learning approaches throughout time. This review will also concentrate on the use of machine learning and artificial intelligence in glaucoma diagnosis. Researchers have made significant progress in creating automatic and accurate glaucoma diagnosis systems by using massive datasets and deep learning approaches. Our goal is to get significant insights into the present state-of-the-art glaucoma diagnosis by thoroughly reviewing numerous research papers, articles, and studies. This comprehensive analysis aims to identify possible areas for further growth and advancement in the field of glaucoma detection.

Shubham Joshi et al. [6] utilized a supervised learning framework model to differentiate glaucoma retinal images from non-glaucoma retinal images. The Computer-Aided Design (CAD) method was used to compute the structural characteristics of the OD and OC regions of the retinal pictures. After that, an ensemble-based learning model was suggested in this study to classify the computed structural features from both the OD and the OC. Finally, the authors classified the glaucomatous retinal pictures using the calculated structural features by employing three distinct deep-learning models previously trained on the data. The identification of glaucoma illnesses through optical tomography retinal images was carried out by Singh et al. [7]. To identify the glaucomatous changes in the retinal pictures, the authors utilized enhanced fine-tuning in conjunction with pre-trained classification framework models. The authors evaluated how well their model performed compared to other pre-trained models.

Glaucoma disease identification and evaluation framework models were presented by Rutuja Shinde et al. [8] to identify glaucoma-impacted retinal pictures. The authors utilized a lightweight LeNET CNN model to classify the glaucoma retinal images and the non-glaucoma retinal images. Additionally, a U-Net model was developed to segment the affected Region of Interest (RoI) from the retinal images to evaluate further the severity levels of the Glaucoma case retinal images. Deep learning technology was used by Ajitha et al. [9] to differentiate glaucomatous retinal images from healthy retinal images. The CNN-SVM and CNN-SoftMax methodologies were used by the authors in the construction of the Glaucoma detection model. Compared with the SVM-SoftMax model suggested in this work, the CNN-Support Vector Machine (SVM) classification strategy showed better performance.

The computation of the Glaucoma retinal images from the non-Glaucoma retinal images was done using a feature extraction framework model employed by Guo et al [10]. This work's suggested linear binary classification approach computed the non-linear systematic features from the Glaucoma case retinal images. The proposed model then utilized these characteristics to identify the Glaucoma retinal images. To assess the usefulness of these methods for future severity level estimate processes, the authors conducted tests using a large-scale retinal image dataset to evaluate the proposed methodology. Deep learning was used in the research conducted by Muthamainah et al. [11] to develop a computational model for the diagnosis of glaucoma pathology in retinal pictures. From glaucomatous and non-glaucomatous retinal pictures, the authors extracted and computed texture pattern characteristics as well as morphological structure information. The authors then categorized these computed features using the deep learning model presented in this study. An auto-encoder architectural model was built by Raghavendra et al [12] to identify the glaucomatous retinal pictures. During the course of this research, a new auto-encoder model was developed employing two-layer pre-trained models.

Parashar et al [13] used FAWT to classify glaucoma. FAWT decomposes pre-processed images into sub-band images, and Relief and SBC extract entropies and fractal dimension-based features, respectively. Fisher's LDA ranks feature values. LS-SVM classifies glaucoma stages using higher-rank information. The proposed technique achieved 93.4% classification accuracy on a public glaucoma database. Jiang et al. [14] presented Joint RCNN for optic disc and optic cup segmentation. Attention processes boost glaucoma detection performance. Two subsystems are trained and tested to diagnose glaucoma using fundus images [15]. The first subsystem recognizes the optic disc and cup, mixes them, and extracts physical and positional properties. The second uses transfer learning to analyze glaucoma eye fundus images. Both methods are used to detect glaucoma. Self-ONNs are proposed [16] for early glaucoma detection in fundus pictures and compared to conventional (deep) CNNs (CNNs). The Bit-plane slicing and local binary patterns [17] were used for glaucoma diagnosis using three SVMs for categorization. SVM decisions are fused to classify the input fundus image as normal or glaucoma. Glaucoma detection using a deep convolution neural network [18] uses CLAHE for preprocessing and two segmentation models (EffcientNet+U-Net) were used to segment the optic cup and disc mask. The framework diagnoses glaucoma using the CDR ratio. GANs are used for OD segmentation [19] and taxonomic diversity indices for feature extraction and texture pattern differentiation.

2.1 Overview of the proposed method

The primary goal of this study is to develop and test a CNN-based model capable of diagnosing glaucoma with high accuracy limitations of present detection approaches. Many present approaches may lack the needed accuracy and sensitivity to identify early-stage glaucoma or subtle changes, resulting in missed diagnosis or delayed therapies. The specific techniques may perform well on select datasets, but their ability to produce consistent and reliable findings degrades when applied to various datasets. To detect and diagnose glaucoma, two distinct CNNs are employed. The first CNN is used to categorize glaucoma images from retinal images, while the second CNN is utilized to identify glaucoma stages. Our model is specifically designed to accurately and sensitively detect Glaucoma in retinal images of various resolutions, ensuring robust performance across different image qualities and achieving high accuracy in the diagnosis.

3. Methodology for Glaucoma Detection

This study presents a potential approach for identifying glaucoma by analyzing retinal pictures with the use of a deep learning algorithm. The framework presented for detecting glaucoma comprises two modules that rely on one another: the Retinal Image Classification Module (RICM) and the Retinal Image Diagnosis Module (RIDM). As shown in Figure 2, the CNN module utilizes the RICM classifier to classify the retinal picture as either a normal or a glaucoma

retinal image. The RIDM detects the neuro rim region from the glaucoma retinal image by segmenting OD and OC. The Dual Functional CNN (DFCNN) classifier is proposed to diagnose the severity stages of the glaucoma image based on the feature patterns that are extracted from the neuroretinal rim in the glaucoma image, as illustrated in Figure 2.

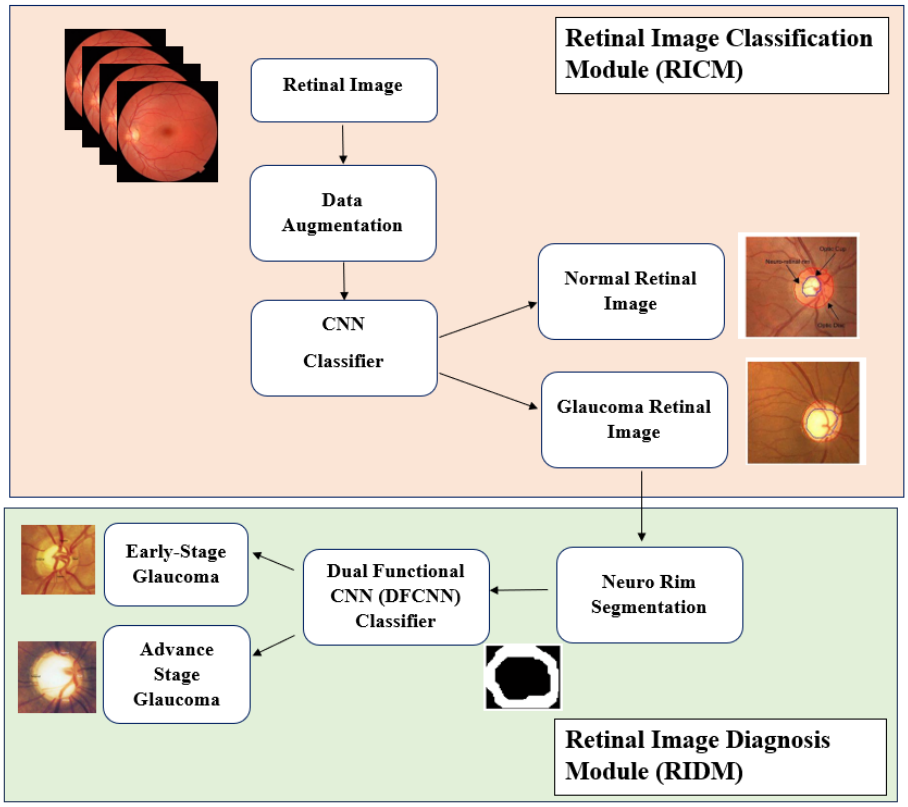

Fig. 2. Flow of the proposed Glaucoma detection and classification method

3.1 Data Augmentation

During the phase of learning where the classification system is being developed, the performance evaluation of the model used for classification mostly depends on the number and quality of the input images. During the learning phase of the classification system, insufficient input photos have the most significant impact on the performance of the suggested system. When it comes to providing excellent performance on the input photos, this is the primary obstacle that the classifier faces. In this article, Data Augmentation, often known as DA, is utilized so that the number and quality of the input images can be improved. The DA is the collection of procedures or functions that, when applied to retinal images, can produce a new set of retinal images by subtly altering the point patterns present in the retinal images used as input. In this article, the DA method is utilized, which can be individually applied to the input retinal images (both normal and Glaucoma retinal images) to increase the quantitative of the input images. These methods include the vertical flip, the horizontal flip, the left scale, and the right scale, as well as contrasting and grey scaling. When you use the vertical and horizontal flip functions, the image that is produced has a point shift of one pixel. The image produced by the left and right scale functions has scales of 0.5. The DA approach, on the other hand, improves contrast by 10% on each pixel. Through the use of the grey scale DA approach, the color retinal image can be transformed into a greyscale image. The data augmented output is shown in figure 3. Table 1 illustrates the outcomes obtained from implementing the DA into practice.

Table 1. Outcomes of DA Implementation

Dataset	Glaucoma images	Glaucoma images after DA	Normal retinal images	Normal retinal images after DA
HRF	15	90	15	90
PAPILA	155	930	333	1998
KAGGLE	1000	6000	1040	6240

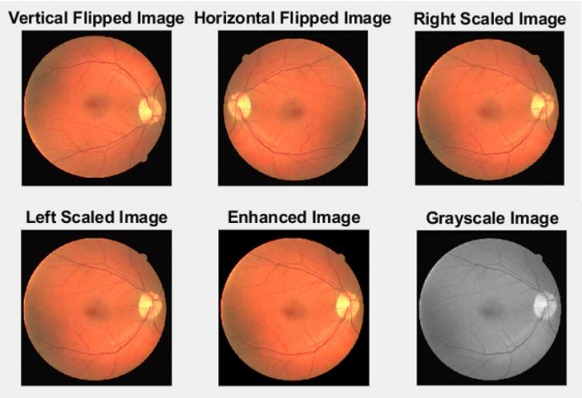

Fig. 3. Output Images after Data Augmentation

3.2 Retinal Image Classification Module (RICM)

The operations of this RICM segment can be broken down into two phases that follow one another: learning and categorization. During the learning phase of RICM, the normal and glaucoma retinal pictures from the database are learned with the help of a data augmentation function, which produces a deep learning matrix (DLM). The CNN classifier with data-augmented retinal images and the DLM pattern, produced by the classifier's learning phase, is utilized in the phase of RICM known as classification. During this phase, the test retinal image that was obtained from the database is classified as either normal or glaucomatous by the CNN classifier. Figure 4 provides a comprehensive explanation of the RICM proposal as a whole.

This article distinguishes glaucomatous retinal images from healthy retinal images by employing a classification framework that is based on deep learning. The retinal images each have unique object patterns, which a machine learning system cannot differentiate straightforwardly. A large number of features are required by the classification algorithm to get a greater glaucoma detection rate. These characteristics are used to differentiate the various object patterns that can be found in retinal images. Based on this, the YOLO architecture, which is an expansion of the CNN architecture, has been employed in this article. Several CNN layers make up the YOLO, and these layers generate a significant number of internal features that are used by the retinal image categorization system.

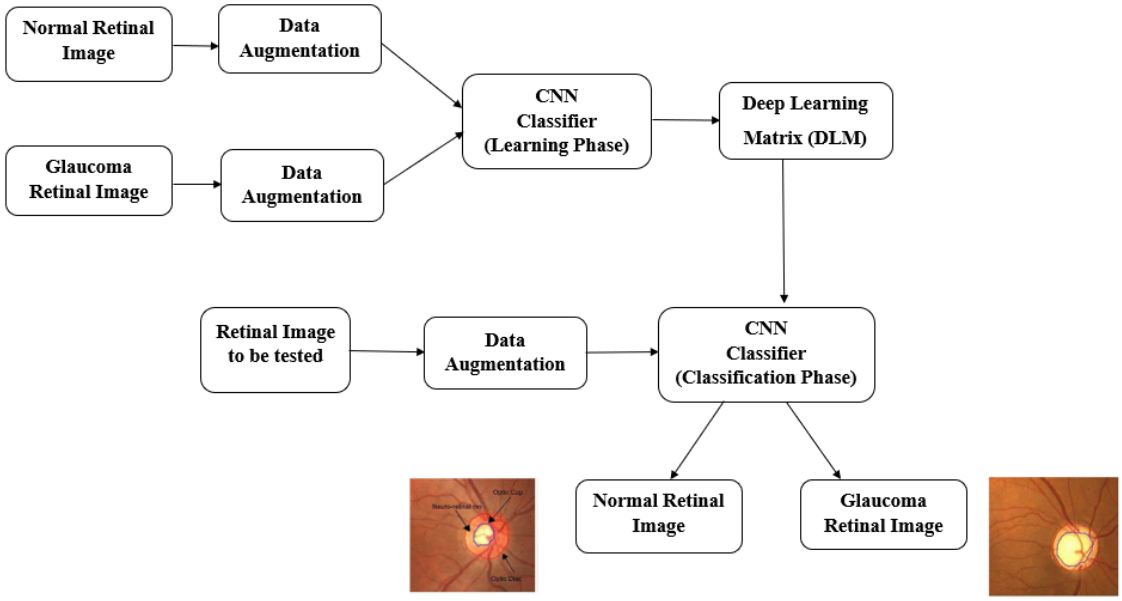

Fig. 4. Retinal Image Classification Module flow diagram

3.2.1 YOLO V5: Glaucoma Detection

The retinal image categorization procedure described in this work makes use of the YOLO-v5 architecture, which is seen in Figure 5. To create this YOLO architecture, five modules of Convolutional Layers (CL) and two modules of Fully Connected Neural Network (FCNN) layers were utilized as building blocks.

Layer 1: The initial Layer 1 module is constructed with 192 CL, and each CL is given a configuration that consists of a 3*3 kernel function.

Layer 2: The second Layer 2 module is built using 128 CL layers that are configured with a 1*1 kernel, 256 CL layers that are set up with a 3*3 kernel, 256 CL layers that are configured with a 1*1 kernel, and 512 CL layers that are configured with a 3*3 kernel, together with two Pooling Layers (PL).

Layer 3: The Third Layer 3 module is created with 4*256 CL layers configured with 1*1 kernel, 4*512 CL layers configured with 3*3 kernel, 512 CL layers configured with 1*1 kernel, 1024 CL layers configured with 3*3 kernel, and two PL. In addition, the module includes two PLs.

Layer 4: The Layer 4 module is constructed with two PL, two 2*1024 CL layers configured with three 3*3 kernels each, two 1024 CL layers configured with three 3*3 kernels each, two 2*1024 CL layers configured with three 3*3 kernels each, and two 2*512 CL layers configured with one 1*1 kernel each. All of these layers are configured with one 512 CL layer each.

Layer 5: The design of the Layer 5 module includes 1024 CL layers configured with a 3*3 kernel and 1024 CL layers configured with a 3*3 kernel and two PLs.

FCNN layer 1 has 4096 neurons, whereas FCNN layer 2 contains just two neurons that correlate to normal or glaucoma classification results.

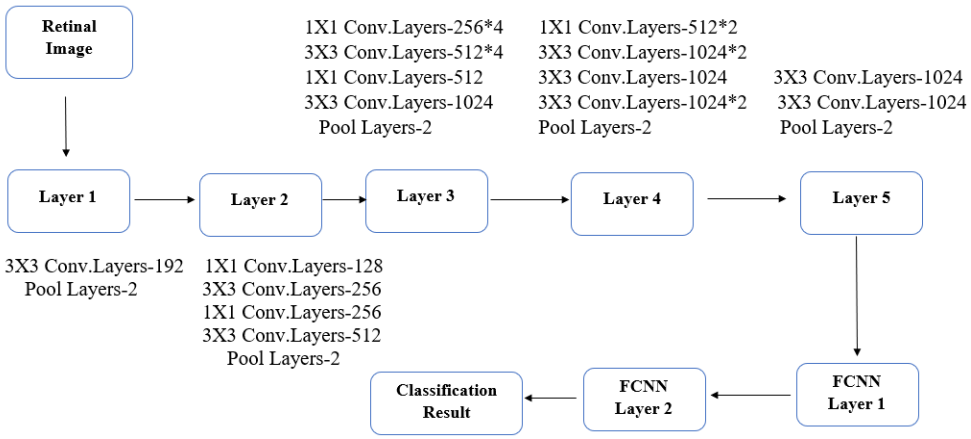

Fig. 5. YOLO architecture for RICM

3.3 Retinal Image Diagnosis Module (RIDM)

Figure 6 provides a visual representation of the RIDM framework for glaucoma severity categorization. Regarding the Training RIDM and Testing RIDM stages, the operation of this suggested framework is described. The suggested Alex Net CNN architecture is used to train the neuro rim region of both the "Early case" and the "Advance case" glaucoma retinal images during the Training RIDM framework. The feature values of Early or Advance case Glaucoma retinal pictures can be computed with the help of this Alex Net CNN architecture. These values come from the Neuro rime region of the images. Estimating the severity levels during Testing RIDM is accomplished by the utilization of a dual CNN architecture. The first CNN architecture is used in the Testing RIDM framework to extract the feature values from the Neuro rim region of the test Glaucoma retinal image. The second CNN architecture is used to classify the computed CNN features into either the "Early" or "Advanced" case Glaucoma retinal images concerning the trained CNN features that are obtained in the Training RIDM framework.

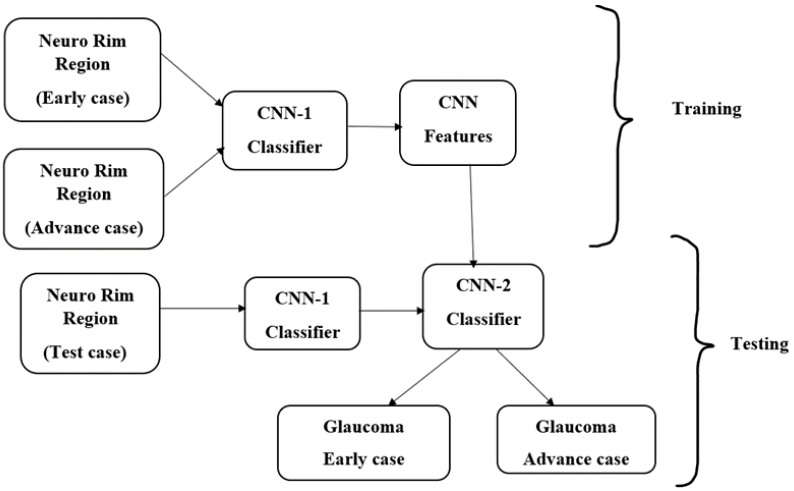

Fig. 6. Retinal Image Diagnosis Module for Glaucoma Severity Classifications

3.3.1 Neurorim Segmentation

The retina is the neural layer/light-sensitive layer of the eye. OD/ONH is the area from which the retinal nerve fibers carrying visual stimulus exist the globe to continue as optic nerve (the 2nd cranial nerve) sending impulses to the visual cortex for processing the image we see. The OD measures about 1.7-1.8mm on average and has a cup in the center that is more pallor than the neuroretinal rim around the cup. The cup is the area through which nerve fibre leaves the globe, and retinal blood vessels enter the eye. The fibers then penetrate the sclera at its lamina cribrosa area which can dip/curve under pressure leading to an increase in the cupping of the disc. Hence measuring the cup disc ratio helps us to detect glaucomatous changes. When the cup size increases there is thinning of the neuro retinal rim. This can further cause retinal nerve fiber layer loss and thinning. The region that lies between the OD and OC is known as the neuro-rim region. This structure of the neuro-rim region is subject to change depending on the ocular pressure. A method known as anisotropic diffusion filtering is utilized to identify the neural rim region that is present in glaucomatous retinal images [20]. An anisotropic diffusion filter is used to segment the neuroretinal margin from the retinal images. This anisotropic filter segmented the neuroretinal rim using four nearby pixels. This work uses anisotropic non-linear diffusion to compute the retinal image's Laplacian and Gradient. The anisotropic diffusion filter has three components: the conductance function, the gradient threshold parameter, and the stopping value. In this study, the non-linear factor is employed as the conductance function, the gradient threshold is set to 0.5 after multiple trials, and the stopping value is set to 100.

Eight retinal images are created by convolving the retinal image with the anisotropic diffusion filter's gradients. The diffused image's maximum pixel is chosen from eight filtered images. The Laplacian index is then utilized to segment the neuroretinal rim. Rim pixels in a diluted image have a higher intensity than other pixels. Figure 7(a) displays the retinal picture, 7(b) shows the diffused image and 7(c) shows the segmented Neuro rim region. The discovered neural rim region is then used in the RIDM step of the diagnostic process to determine the severity levels of the Glaucoma condition.

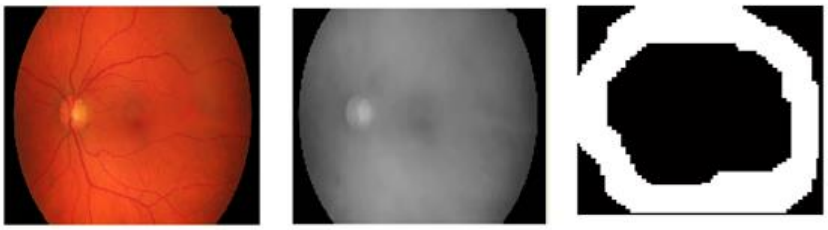

(a) (b) (c)

Fig. 7. Neurorim segmentation: (a) Retinal image (b) Diffused image (c) Neuro rim region segmented by the proposed method

3.3.2 Alexnet: Glaucoma Severity Diagnosis

The traditional Alex Net CNN architecture consisted of eight internal layers, each of which had learnable parameter configurations. There were five CL layers and three FCNN levels. The configuration of all eight of these internal layers is in the form of a series, with the final FCNN layer being the one that generates the severity levels. The CNN-1 architecture is comprised of five CL modules, the first of which is configured with 96 filters, the second of which is configured with 256 filters, the third and fourth of which are configured with 384 filters each, and the fifth of which is configured with 256 filters. These configurations are depicted in figure 8, which can be found here (a). To generate the feature maps, the CNN-1 architecture is provided with input from the Neuro rim region of both the Early and advanced examples. The CNN-1 architecture is responsible for generating these feature maps, which are then classified using the CNN-2 architecture. The CNN-2 architecture, which is shown in figure 8b, is an expansion of the CNN-1 architecture that includes three FCNN layers. Fig. 8b depicts this extension. The 'Early' and 'Advanced' stages are shown by the fact that the third FCNN layer only contains two neurons, while the first two FCNN layers have a total of 4096 neurons.

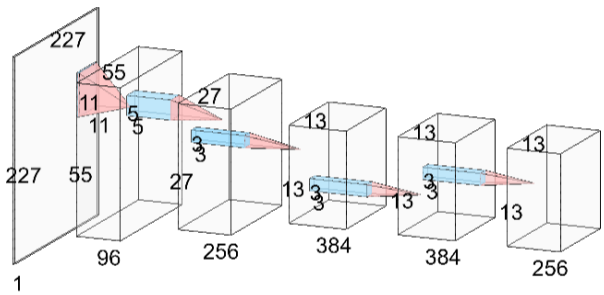

(a) CNN-1 architecture for feature computations

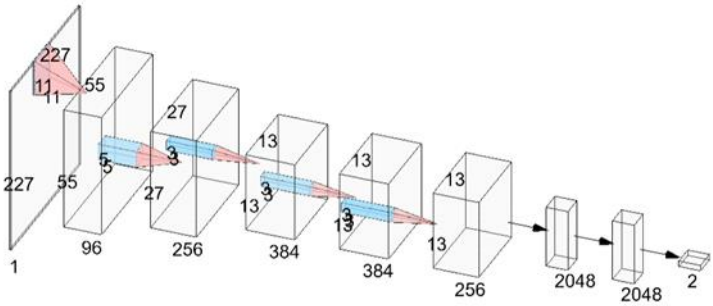

(b) CNN-2 architecture for feature classifications

Fig. 8. Dual Functional CNN architectures

4. Result and Discussion

Dataset	Healthy Images	Glaucoma Images
PAPILA	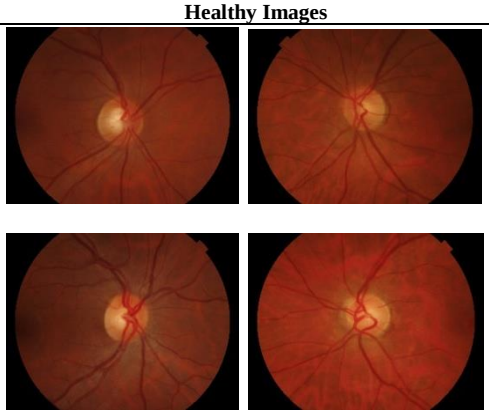	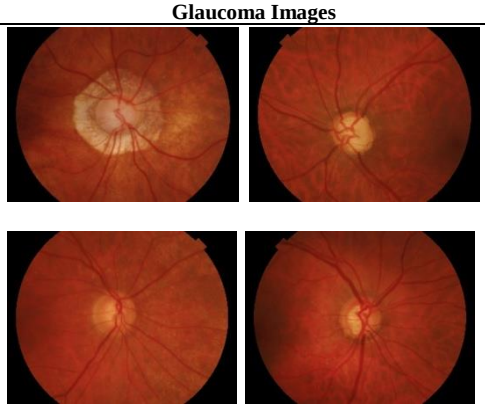
HRF	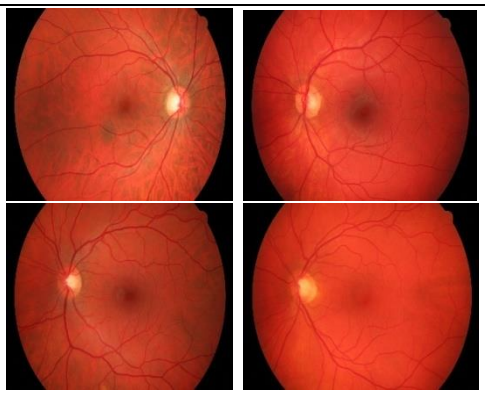	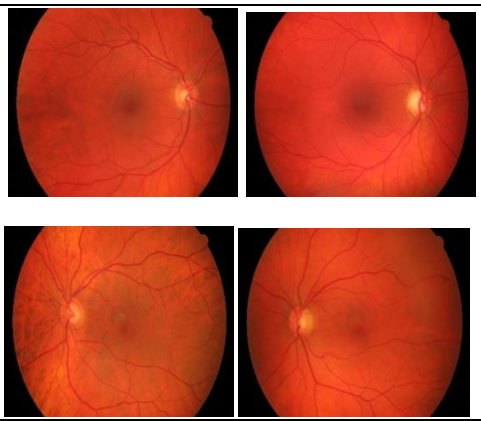
KAGGLE	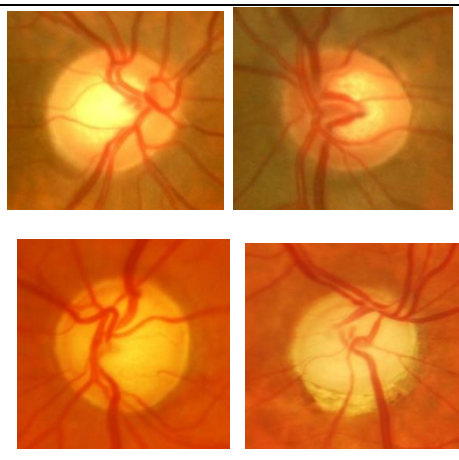	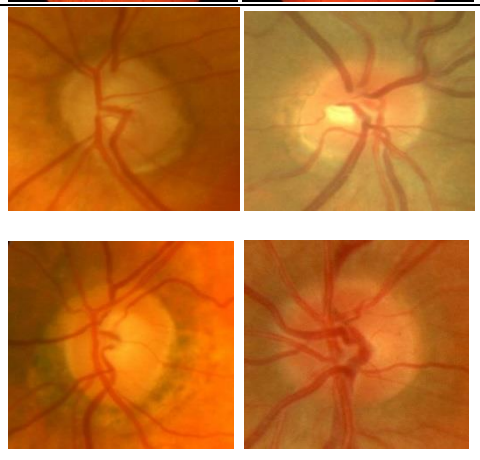

Fig. 9. Sample images from the datasets

To evaluate the performance of the proposed method, two datasets are used. HRF dataset (High-Resolution Images) was developed and kept up to date by the Department of Ophthalmology at Friedrich-Alexander University in Germany. The retinal images are collected in the age group between 25 and 70 from Germany. A total of 15 healthy images and 15 glaucoma images are included in the HRF collection. Each of these images has a high resolution of 3504 × 2336. In this collection, experienced ophthalmologists have provided masks and their respective fields of view (FoV) for every retinal image. The CR-1 fundus camera, which has a field of view of 45 degrees, was used to acquire the retinal pictures that are included in this collection [21]. Ophthalmologists reviewed every one of the retinal images to ensure their accuracy. The Department of Ophthalmology at General University Hospital in Spain collected the retinal pictures included in the PAPILA dataset (Low-Resolution Images). The patients' retinas are imaged sometime between the years 2018 and 2020 throughout the data collection process. The retinal pictures included in this dataset were divided into two groups, which were then given the designations Group 1 and Group 2. Glaucoma is represented by the retinal pictures in Group 1, while normal vision is represented by the retinal images in Group 2. The patient's age from 14 to 90 and gender information are included in each record. A Topcon TRC-NW400 non-mydriatic retinal camera, which has a resolution of 2576×1934 pixels, was utilized by an ophthalmologist to capture these images. This dataset consists of 333 normal retinal images and 155 glaucoma retinal images; both sets of photos have been checked for accuracy by ophthalmologists with advanced training [22,23]. The sample images from both resolution datasets are shown in Figure 9.

Moreover, the Kaggle dataset [30] has been used in this paper to show the performance efficiency of the proposed methodology on a large number of retinal images. This dataset contains 2040 retinal images in the category of Glaucoma images (1000) and Healthy case retinal images (1040). In addition, this dataset also contains the gold standard images to compare the proposed method's performance efficiency. The retinal images in this dataset are collected through the CCD camera equipment from the age group between 30 and 70 and the acquisition of the retinal images was carried out in the UK demographic area. Among the 1000 numbers of Glaucoma retinal images, 450 images are in the category of Early case and the remaining 650 retinal images are in the category of Advance.

The following metric indexes are used in this article to validate the performance efficiency of the proposed Glaucoma detection system.

$$Glaucoma\ Detection\ Metric\ (GDM) = \left(\frac{Correctly\ detected\ Glaucoma\ images\ count}{N1}\right) \quad (1)$$

$$Healthy\ Retinal\ Detection\ Metric\ (HRDM) = \left(\frac{Correctly\ detected\ healthy\ retinal\ images\ count}{N2}\right) \quad (2)$$

where N1 and N2 are the total Glaucoma and healthy retinal images in the dataset.

The GDM and HRDM are both calculated as a percentage, and their values can range anywhere from 0 to 100. If the GDM and HRDM values are low, this indicates that the proposed glaucoma detection system achieves a lower level of efficiency, whereas if the GDM and HRDM values are high, this indicates that the proposed glaucoma detection system achieves a higher level of efficiency.

The glaucoma detection system that has been proposed finds 14 glaucoma images out of a total of 15 glaucoma images, and it also finds 15 healthy retinal images out of a total of 15 healthy retinal images from the HRF dataset, as shown in Figure 10(a). Because of this, the suggested technique achieves a GDM of 93.3% and an HRDM of 100%, resulting in an average Glaucoma detection index of around 96.6%. In the PAPILA dataset, the proposed Glaucoma detection system can recognize healthy retinal images, which is an improvement over 333 healthy retinal photos (as shown in Figure 10(b)). Additionally, it can detect 153 Glaucoma images, which is an improvement over 155 Glaucoma images. As a result, the suggested approach achieves a GDM of 98.7% and an HRDM of 97.2%, with an overall Glaucoma detection index of around 97.9%.

In the case of the Kaggle dataset [30], the glaucoma detection system that has been proposed finds 987 glaucoma images out of a total of 1000 glaucoma images, and it also finds 1040 healthy retinal images out of a total of 1040 healthy retinal images from the Kaggle dataset. Because of this, the suggested technique achieves a GDM of 98.7% and an HRDM of 100%, resulting in an average Glaucoma detection index of around 99.35%.

Table 2 shows the impact of data augmentation on the Glaucoma retinal image detection process for the performance evaluation parameters GDM and HRDM on different retinal imaging datasets.

Table 2. Impact of data augmentation on Glaucoma retinal images detection process

Dataset	Without data augmentation		With data augmentation	
	GDM (%)	HRDM (%)	GDM (%)	HRDM (%)
HRF	90.7	96.3	93.3	100
PAPILA	92.9	93.9	98.7	97.2
Kaggle	95.3	96.5	98.7	100

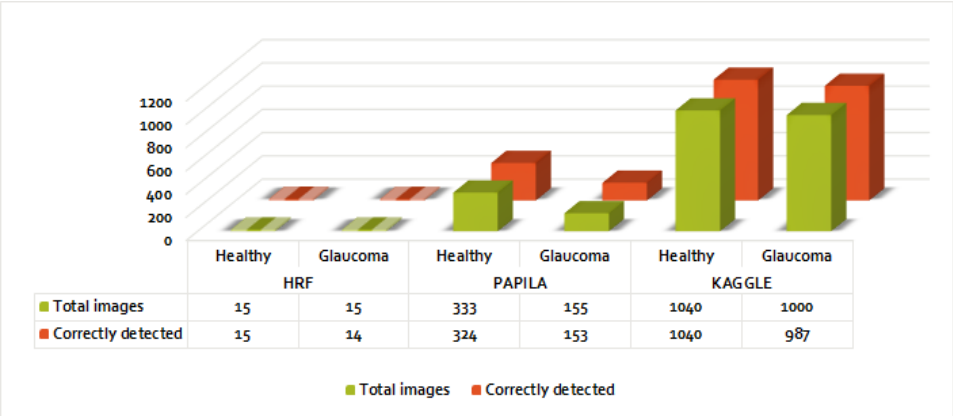

Fig. 10. Performance Metric Output Comparison

The following metrics are utilized in addition to the ones already mentioned for analyzing performance in this article.

$$Sensitivity\ (Se) = \frac{TP}{TP+FN} \tag{3}$$

$$Specificity\ (Sp) = \frac{TN}{FP+TN} \tag{4}$$

$$Accuracy\ (Acc) = \frac{TP+TN}{TP+TN+FP+FN} \tag{5}$$

Pixels in retinal pictures that are correctly identified as being either OD or non-OD are denoted by TP and TN, respectively, whereas those that are incorrectly identified are denoted by FP and FN.

The stagewise segmentation output starting from the fundus images to the Optic Disc and Optic Cup segmented output is shown in figure 11. Figure 12a depicts the segmented optic band, and Figure 12b demonstrates the segmented optic band's four distinct quadrants.

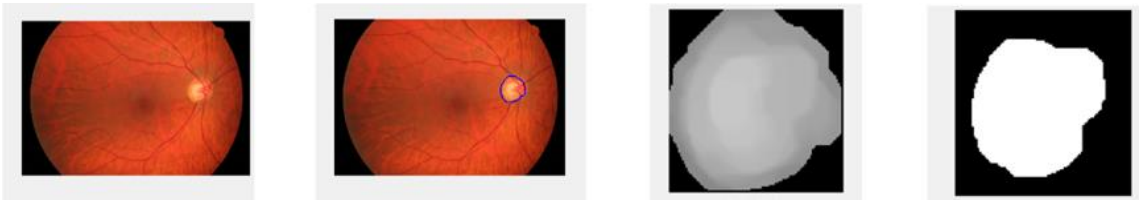

(a) (b) (c) (d)

Fig. 11. Stagewise Segmentation output: (a) Input Fundus Image (b) Optic Disc Image (c) Segmented OD (d) Segmented OC

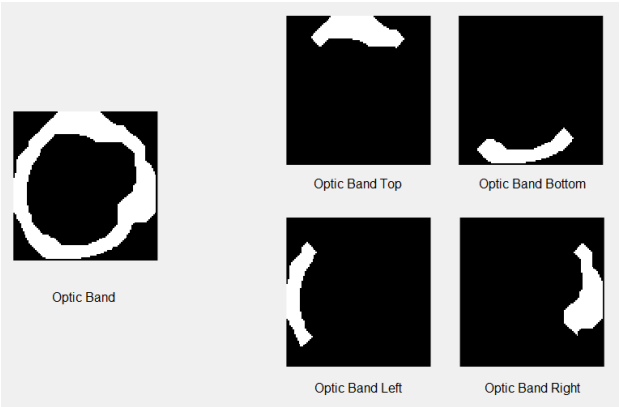

(a) (b)

Fig. 12. (a) Segmented Optic Band (b) Four different quadrants of segmented Optic Band

Table 3 shows that for the Glaucoma retinal pictures in the PAPILA dataset, the proposed Glaucoma detection method in this study obtains 98.77% Se, 98.74% Sp, and 98.62% Acc, for the HRF dataset 98.58% Se, 98.62% Sp, and 98.83% Acc, and for the KAGGLE dataset 99.16%Se, 99.27% Sp and 98.96% Acc.

Table 3. Analysis of the dataset for Optical Disc segmentation

Glaucoma retinal images	PAPILA			HRF			KAGGLE		
	Se (%)	Sp (%)	Acc (%)	Se (%)	Sp (%)	Acc (%)	Se (%)	Sp (%)	Acc (%)
1	98.3	99.3	98.3	98.3	98.4	98.3	99.3	99.1	98.7
2	98.2	98.8	98.2	98.8	98.2	98.8	99.5	99.4	99.3
3	98.4	98.4	99.4	99.1	98.6	99.2	98.9	99.5	98.7
4	99.2	98.2	99.1	99.3	98.2	99.7	99.3	99.3	98.7
5	99.3	99.4	98.3	98.2	99.3	98.4	98.5	99.4	99.2
6	98.8	98.8	98.9	98.7	99.2	98.9	99.3	99.3	99.5
7	99.4	98.3	97.9	98.3	98.8	98.4	98.7	98.9	98.7
8	98.7	98.2	99.2	98.2	98.3	98.7	99.3	99.5	99.4
9	98.3	99.1	98.6	98.6	98.4	98.8	99.3	99.2	98.7
10	99.1	98.9	98.3	98.3	98.8	99.1	99.5	99.1	98.7
Average values	**98.77**	**98.74**	**98.62**	**98.58**	**98.62**	**98.83**	**99.16**	**99.27**	**98.96**

Tables 4,5 and 6 show the performance analysis of Neuro rim segmentation on the PAPILA, HRF, and KAGGLE datasets concerning Neuro rim top, Neuro rim bottom, Neuro rim left, and Neuro rim right, respectively.

Table 4. Performance analysis of Neuro rim segmentation on the PAPILA dataset

Retinal Image	Experimental results in %											
	Neuro rim Top			Neuro rim bottom			Neuro rim Left			Neuro rim right		
	Se	Sp	Acc	Se	Sp	Acc	Se	Sp	Acc	Se	Sp	Acc
1	98.3	98.4	98.5	98.4	98.8	98.4	98.6	98.4	99.3	98.4	98.7	98.7
2	98.2	98.2	98.2	98.2	98.7	98.2	98.4	98.3	98.7	99.8	99.3	98.3
3	98.5	98.5	99.1	98.6	98.5	98.8	99.2	99.2	98.6	98.7	98.7	98.8
4	99.2	98.3	98.9	98.7	99.3	99.3	99.1	98.9	98.4	98.7	98.5	98.2
5	98.3	98.1	98.3	99.3	99.7	98.9	98.9	98.4	99.1	99.3	99.3	98.9
6	98.4	98.9	99.2	99.1	99.0	98.2	98.4	98.5	99.4	99.2	98.7	98.4
7	98.1	99.2	98.7	98.7	98.6	99.4	98.2	98.9	98.8	99.7	99.5	98.3
8	99.5	99.1	98.6	98.9	98.9	99.2	98.7	99.2	98.7	98.7	99.3	98.9
9	99.2	98.4	98.4	99.3	98.7	98.7	99.3	98.6	98.9	98.6	98.7	99.3
10	99.1	98.2	98.1	98.2	99.1	98.6	98.7	98.7	98.4	98.5	98.7	99.1
Average	**98.6**	**98.5**	**98.6**	**98.7**	**98.9**	**98.7**	**98.7**	**98.7**	**98.8**	**98.9**	**98.9**	**98.6**

Table 5. Performance analysis of Neuro rim segmentation on the HRF dataset

Retinal Image	Experimental results in %											
	Neuro rim Top			Neuro rim bottom			Neuro rim Left			Neuro rim right		
	Se	Sp	Acc	Se	Sp	Acc	Se	Sp	Acc	Se	Sp	Acc
1	98.8	98.6	99.3	99.3	98.5	99.3	98.8	98.2	99.4	98.7	99.3	98.4
2	99.2	98.3	99.1	99.1	99.3	98.6	98.6	98.7	98.8	99.3	99.1	98.9
3	99.1	98.2	98.9	98.8	99.6	98.6	99.3	98.4	99.1	99.1	98.8	98.3
4	98.7	99.7	98.3	98.6	98.7	98.9	98.7	99.3	98.7	98.7	98.3	98.7
5	98.7	98.6	99.2	98.4	98.6	98.6	98.9	99.1	98.3	98.4	98.7	98.2
6	98.5	98.5	98.6	98.7	98.9	98.4	99.5	98.9	98.7	98.8	98.4	99.1
7	99.3	99.3	98.7	98.3	98.5	98.2	99.1	98.7	98.4	98.9	98.2	99.3
8	98.7	99.1	98.4	98.7	98.7	99.1	98.9	99.3	99.2	98.4	98.6	98.8
9	98.2	98.5	98.3	98.4	98.9	98.8	98.3	99.1	99.5	98.3	98.4	98.6
10	99.7	98.7	98.9	98.1	99.4	98.7	98.7	99.6	98.6	98.7	98.2	98.8
Average	**98.8**	**98.7**	**98.7**	**98.6**	**98.9**	**98.7**	**98.8**	**98.9**	**98.8**	**98.7**	**98.6**	**98.7**

Table 6. Performance analysis of Neuro rim segmentation on the Kaggle dataset

Retinal Image	Experimental results in %											
	Neuro rim Top			Neuro rim bottom			Neuro rim Left			Neuro rim right		
	Se	Sp	Acc	Se	Sp	Acc	Se	Sp	Acc	Se	Sp	Acc
1	98.8	99.3	98.4	98.9	98.4	99.3	98.4	98.5	98.7	98.3	98.7	98.6
2	99.3	99.2	98.7	98.3	98.9	99.1	99.3	98.3	98.4	98.2	98.4	98.4
3	99.2	98.5	98.9	99.2	99.3	98.9	99.9	98.2	99.3	98.7	98.6	99.2
4	98.9	98.3	99.3	99.9	99.2	98.3	98.7	98.9	99.3	99.1	98.9	98.5
5	98.6	98.7	99.2	98.5	99.6	98.6	98.5	98.5	98.8	99.3	99.3	98.7
6	99.2	98.4	99.7	98.3	98.9	98.4	98.7	99.3	98.4	98.2	99.2	98.4
7	99.4	99.3	99.2	98.2	99.3	99.3	98.5	99.2	99.4	98.7	99.5	98.3
8	98.7	99.2	99.3	98.9	98.5	99.2	98.3	99.9	99.2	98.6	98.5	98.7
9	98.9	98.5	98.9	98.4	98.0	98.8	98.9	98.5	99.8	98.5	98.3	99.3
10	99.3	98.2	98.5	98.3	99.3	98.7	98.4	98.3	99.3	98.3	98.6	99.7
Average	**99.03**	**98.76**	**99.01**	**98.69**	**98.94**	**98.86**	**98.76**	**98.76**	**99.06**	**98.59**	**98.8**	**98.78**

Table 7 shows the comparative analysis of OD segmentation on the PAPILA dataset with other state-of-the-art methods. The proposed method obtained higher results from these evaluation and comparison results concerning other methods on PAPILA dataset retinal images.

Table 7. Analysis of state-of-the-art algorithms for OD segmentation on the PAPILA dataset

Authors	Deep learning Methods	Se (%)	Sp (%)	Acc (%)
The proposed approach	**DFCNN classifier**	**98.77**	**98.74**	**98.62**
Morales et al [24]	Assembling Deep Networks	78%	81%	74%
Hemelings et al [25]	Generalizable deep learning regression model	81.3%	78%	70%

Table 8 displays the results of a comparison of state-of-the-art OD segmentation techniques on the HRF dataset. The results produced using the proposed method on the HRF dataset retinal pictures were found to be superior to those acquired using the other methods evaluated and compared.

Table 8. Analysis of state-of-the-art algorithms for OD segmentation on the HRF dataset

Authors	Deep learning Methods	Se (%)	Sp (%)	Acc (%)
The proposed approach	**DFCNN classifier**	**98.58**	**98.62**	**98.83**
Akbar et al [26]	Deep transfer learning approach	93.3%	88.46%	89.3%
Hamid et al [27]	AlexNet- deep learning algorithm	93.3%	90.9%	96.7%
Nazir et al [28]	Improved mask-RCNN	96.5%	96.3%	96.5%
Latif et al [29]	ODGNet	91.7%	91.3%	92.2%

Table 9 displays the results of a comparison of state-of-the-art OD segmentation techniques on the Kaggle dataset. The results produced using the proposed method on the Kaggle dataset retinal pictures were found to be superior to those acquired using the other methods evaluated and compared.

Table 9. Analysis of state-of-the-art algorithms for OD segmentation on the Kaggle dataset

Authors	Deep learning Methods	Se (%)	Sp (%)	Acc (%)
The proposed approach	**DFCNN classifier**	**99.2**	**99.3**	**98.96**
Akbar et al [26]	Deep transfer learning approach	93.3%	88.46%	89.3%
Hamid et al [27]	AlexNet-deep learning algorithm	93.3%	90.9%	96.7%
Nazir et al [28]	Improved mask-RCNN	96.5%	96.3%	96.5%
Latif et al [29]	ODGNet	91.7%	91.3%	92.2%

For analyzing the error of the neurorim segmentation, the experimental results of the segmented neurorim region (x) by the proposed method have been compared with the gold standard neuro rim region (y) which are available in the dataset. To find the error analysis, Root Mean Square (RMS) has been computed between ‘x’ and ‘y’ and they are given in the following Table 10 and Table 11 shows the comparisons of RMS analysis with other state of art methods.

Table 10. Error analysis on different retinal imaging datasets

Datasets	RMS
HRF	0.061
PAPILA	0.025
Kaggle	0.032

Table 11. Comparisons of RMS analysis on other state of art methods

Datasets	RMS		
	Proposed work (in this paper)	Akbar et al [26]	Hamid et al [27]
HRF	0.061	0.287	0.378
PAPILA	0.025	0.165	0.652
Kaggle	0.032	0.743	0.676

Glaucoma Diagnosis Rate (GDR) is a parameter that is defined as the ratio between the correctly diagnosed Glaucoma images and the total Glaucoma images considered in each case. It is measured in percentage and the system performance is high if GDR is having high value. The GDR is depicted in the following equation.

$$GDR\ (\%) = \frac{\text{Correctly diagnosed Glaucoma images}}{\text{Total Glaucoma images considered in each case}} \quad (6)$$

Along with the GDR, morphological parameters Area, width, height, Perimeter, and eccentricity, are computed from the segmented neurorim region in the classified Glaucoma retinal image. These morphological parameters along with the GDR from the Early case and Advance case, are fed into the Dual CNN classifier for producing the trained patterns. During testing of the proposed diagnosis method, the morphological parameters along with GDR from the test Glaucoma retinal image are fed along with the trained patterns to the proposed Dual CNN classifier to produce the diagnosis results.

The HRF dataset has 15 Glaucoma retinal images, and these images are further categorized into 10 'Early' cases and 5 'Advanced' cases images. The proposed system stated in this paper correctly diagnosed 9 'Early' case images over 10 'Early' case images; hence, the GDR for Early cases is about 90%. The proposed system stated in this paper correctly diagnosed 5 'Advance' case images over 5 'Advance' case images; hence, the GDR for Advanced case is about 100%. Hence, the average GDR for the retinal images in the HRF dataset is about 95%.

The PAPILA dataset has 155 Glaucoma retinal images, and these images are further categorized into 140 'Early' cases and 15 'Advanced' case images. The proposed system stated in this paper correctly diagnosed 138 'Early' case images over 140 'Early' case images; hence, the GDR for Early cases is about 98.5% as shown in figure 13. The proposed system stated in this paper correctly diagnosed 14 'Advance' case images over 15 'Advance' case images; hence, the GDR for the Advance case is about 93.3%. Hence, the average GDR for the retinal images in the PAPILA dataset is about 95.9%.

The Kaggle dataset has 1000 Glaucoma retinal images, and these images are further categorized into 450 'Early' cases and 550 'Advanced' case images. The proposed system stated in this paper correctly diagnosed 443 'Early' case images over 450 'Early' case images; hence, the GDR for Early cases is about 98.4%. The proposed system stated in this paper correctly diagnosed 547 'Advance' case images over 550 'Advance' case images; hence, the GDR for the Advance case is about 99.5%. Hence, the average GDR for the retinal images in the Kaggle dataset is about 98.9%.

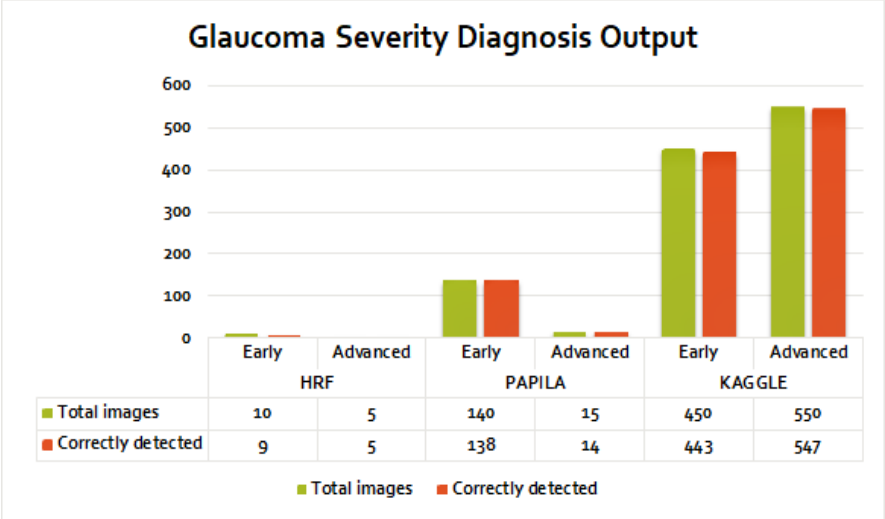

Fig. 13. Glaucoma Diagnosis Rate Output Performance

5. Conclusion

Early identification of glaucoma is critical since it can assist in early diagnosis, preventing the illness from spreading further. We developed a simple yet successful technique for detecting glaucoma from fundus images in this paper. The YOLO deep learning approach is employed in this proposed method for the detection of glaucoma retinal images, and the proposed CNN method is used to evaluate the severity levels of the glaucoma retinal images that have been detected. On the PAPILA dataset's retinal pictures, the proposed method achieves a GDM detection rate of 98.7%, an HRDM detection rate of 97.2%, and an average Glaucoma detection index of about 97.9%. On HRF dataset retinal pictures, the proposed method achieves a GDM detection rate of 93.3% and an HRDM detection rate of 100%, with an average glaucoma detection index of approximately 96.6% and for the KAGGLE dataset retinal pictures, the proposed method achieves a GDM detection rate of 98.7% and an HRDM detection rate of 100%, with an average glaucoma detection index of approximately 99.35%. The proposed Glaucoma detection method described in this article achieves a sensitivity of 98.77%, a specificity of 98.74%, and an accuracy of 98.62% for the retinal images in the PAPILA dataset. Additionally, the proposed Glaucoma detection method achieves a sensitivity of 98.58%, a specificity of 98.62%, and an accuracy of 98.83% for the HRF dataset and a sensitivity of 99.2%, a specificity of 99.3%, and an accuracy of 98.96% for KAGGLE dataset. Therefore, the model that was proposed will be of great help in patients unable to undergo automated perimetry due to any issues so we can detect glaucoma early. This method will also help the ophthalmologist to speed up the process of identifying the stages of glaucoma.

Acknowledgment

We would like to thank Dr. V. K. Smitha, Assistant Professor, Department of Ophthalmology, SRM Medical College Hospital & Research Centre, Kattankulathur for validating the results.

Data Availability Statement

The data that support the findings of this study are openly available in

i. HRF dataset: https://www5.cs.fau.de/research/data/fundus-images
ii. PAPILA dataset: https://doi.org/10.6084/m9.figshare.14798004.v1

Funding Statement

No external funding sources supported this research article.

Conflict of Interest

All authors declare that they have no conflicts of interest.

Ethics Approval Statement

There are no human participants in this article, and informed consent is not applicable

References

[1] Das, P., Nirmala, S.R. and Medhi, J.P., 2016. Diagnosis of glaucoma using CDR and NRR area in retina images. Network Modeling Analysis in Health Informatics and Bioinformatics, 5, pp.1-14.

[2] Senthil, S., Nakka, M., Sachdeva, V., Goyal, S., Sahoo, N. and Choudhari, N., 2021, November. Glaucoma Mimickers: A major review of causes, diagnostic evaluation, and recommendations. In Seminars in Ophthalmology Vol. 36, No. 8, pp. 692-712.

[3] Tham, Y.C., Li, X., Wong, T.Y., Quigley, H.A., Aung, T. and Cheng, C.Y., 2014. Global prevalence of glaucoma and projections of glaucoma burden through 2040: a systematic review and meta-analysis. Ophthalmology, 121(11), pp.2081-2090..

[4] Gupta, N., Garg, H. and Agarwal, R., 2021. A robust framework for glaucoma detection using CLAHE and EfficientNet. The Visual Computer, pp.1-14.

[5] David, D. Stalin, S. Selvi, S. Sivaprakash, P. Vishnu Raja, Dilip Kumar Sharma, Pankaj Dadheech, and Sudhakar Sengan, 2022 Enhanced Detection of Glaucoma on Ensemble Convolutional Neural Network for Clinical Informatics Computers, Materials & Continua 70, no. 2.

[6] Joshi, S., Partibane, B., Hatamleh, W.A., Tarazi, H., Yadav, C.S. and Krah, D., 2022. Glaucoma detection using image processing and supervised learning for classification. Journal of Healthcare Engineering, 2022, 2988262

[7] Singh, L.K., Pooja, Garg, H. and Khanna, M., 2022. Performance evaluation of various deep learning-based models for effective glaucoma evaluation using optical coherence tomography images. Multimedia Tools and Applications, 81(19), pp.27737-27781.

[8] Shinde, R., 2021. Glaucoma detection in retinal fundus images using U-Net and supervised machine learning algorithms. Intelligence-Based Medicine, 5, p.100038.

[9] Ajitha, S., Akkara, J.D. and Judy, M.V., 2021. Identification of glaucoma from fundus images using deep learning techniques. Indian journal of ophthalmology, 69(10), p.2702.

[10] Guo, F., Li, W., Tang, J., Zou, B. and Fan, Z., 2020. Automated glaucoma screening method based on image segmentation and feature extraction. Medical & Biological Engineering & Computing, 58, pp.2567-2586.

[11] Muthmainah, M.U., Nugroho, H.A. and Winduratna, B., 2019, Glaucoma classification based on texture and morphological features. In 5th international conference on science and technology (ICST), IEEE (Vol. 1, pp. 1-6).

[12] Raghavendra, U., Gudigar, A., Bhandary, S.V., Rao, T.N., Ciaccio, E.J. and Acharya, U.R., 2019. A two layer sparse autoencoder for glaucoma identification with fundus images. Journal of medical systems, 43, pp.1-9.

[13] Parashar, D. and Agrawal, D.K., 2020. Automated classification of glaucoma stages using flexible analytic wavelet transform from retinal fundus images. IEEE Sensors Journal, 20(21), pp.12885-12894.

[14] Jiang, Y., Duan, L., Cheng, J., Gu, Z., Xia, H., Fu, H., Li, C. and Liu, J., 2019. JointRCNN: a region-based convolutional neural network for optic disc and cup segmentation. IEEE Transactions on Biomedical Engineering, 67(2), pp.335-343.

[15] Civit-Masot, J., Domínguez-Morales, M.J., Vicente-Díaz, S. and Civit, A., 2020. Dual machine-learning system to aid glaucoma diagnosis using disc and cup feature extraction. IEEE Access, 8, pp.127519-127529.

[16] Devecioglu, O.C., Malik, J., Ince, T., Kiranyaz, S., Atalay, E. and Gabbouj, M., 2021. Real-time glaucoma detection from digital fundus images using self-onns. IEEE Access, 9, pp.140031-140041.

[17] Kanhangad, V. and Pachori, R.B., 2019. Automated glaucoma diagnosis using bit-plane slicing and local binary pattern techniques. Computers in Biology and Medicine, 105, 72-80.

[18] Gupta, N., Garg, H. and Agarwal, R., 2021. A robust framework for glaucoma detection using CLAHE and EfficientNet. The Visual Computer, pp.1-14.

[19] Tomaz Ribeiro Viana Bisneto, Antonio Oseas de Carvalho Filho, Deborah Maria Vieira Magalhães, 2020 Generative adversarial network and texture features applied to automatic glaucoma detection, Applied Soft Computing, Volume 90, 106165

[20] Palma, C.A., Cappabianco, F.A., Ide, J.S. and Miranda, P.A., 2014. Anisotropic diffusion filtering operation and limitations-magnetic resonance imaging evaluation. IFAC Proceedings Volumes, 47(3), pp.3887-3892.
[21] HRF dataset: https://www5.cs.fau.de/research/data/fundus-images
[22] Kovalyk, O., Morales-Sánchez, J., Verdú-Monedero, R., Sellés-Navarro, I., Palazón-Cabanes, A. and Sancho-Gómez, J.L., 2022. PAPILA: Dataset with fundus images and clinical data of both eyes of the same patient for glaucoma assessment. Scientific Data, 9(1), p.291.
[23] PAPILA dataset: https://doi.org/10.6084/m9.figshare.14798004.v1
[24] Sánchez-Morales, A., Morales-Sánchez, J., Kovalyk, O., Verdú-Monedero, R. and Sancho-Gómez, J.L., 2022. Improving Glaucoma Diagnosis Assembling Deep Networks and Voting Schemes. Diagnostics, 12(6), p.1382.
[25] Hemelings, R., Elen, B., Schuster, A.K., Blaschko, M.B., Barbosa-Breda, J., Hujanen, P., Junglas, A., Nickels, S., White, A., Pfeiffer, N. and Mitchell, P., 2023. A generalizable deep learning regression model for automated glaucoma screening from fundus images. NPJ Digital Medicine, 6(1), p.112.
[26] Akbar, S., Hassan, S.A., Shoukat, A., Alyami, J. and Bahaj, S.A., 2022. Detection of microscopic glaucoma through fundus images using deep transfer learning approach. Microscopy Research and Technique, 85(6), pp.2259-2276.
[27] Abdel-Hamid, L., 2020. Glaucoma detection from retinal images using statistical and textural wavelet features. Journal of digital imaging, 33(1), pp.151-158.
[28] Nazir, T., Irtaza, A. and Starovoitov, V., 2021. Optic disc and optic cup segmentation for glaucoma detection from blur retinal images using improved mask-RCNN. International Journal of Optics, 2021, pp.1-12.
[29] Latif, J., Tu, S., Xiao, C., Ur Rehman, S., Imran, A. and Latif, Y., 2022. ODGNet: a deep learning model for automated optic disc localization and glaucoma classification using fundus images. SN Applied Sciences, 4(4), p.98.
[30] https://www.kaggle.com/datasets/arnavjain1/glaucoma-datasets

Authors' Profiles

G. Latha received her BE degree in Electronics and Communication Engineering from Anna University, Chennai, in 2005 and her ME degree in Applied Electronics from Anna University, Tiruchirappalli in 2010. She is currently a Ph.D. student at SRM Institute of Science and Technology, Chennai. Her research interests include machine learning, deep learning, and image processing with biomedical applications.

P. Aruna Priya is a teaching faculty for the past 29 years and currently working as a Professor in the Department of Electronics and Communication Engineering at SRM Institute of Science and Technology, Kattankulathur, India. Prof. P. Aruna Priya received her ME degree from the University of Madras in Computer Science and Engineering and Ph.D. Degree in Nano-electronics from SRM University, in 2011. Her research interests include the design of VLSI circuits, Modelling of Nano-devices and circuits, Design and Implementation of Plasmonic Nanoantenna, Intelligent Automation and Processing of Images. She has published more than 80 papers in international journals and conferences. She is a Fellow of IEI and IETE.

How to cite this paper: G. Latha, P. Aruna Priya, "Glaucoma Detection and Severity Diagnosis from Fundus Images Using Dual CNN Architectures", International Journal of Image, Graphics and Signal Processing(IJIGSP), Vol.16, No.6, pp. 17-31, 2024. DOI:10.5815/ijigsp.2024.06.02